Template-assisted bottom-up growth of nanocrystalline diamond micropillar arrays

Frota Sartori, Andre; Overes, Bart; Fanzio, Paola; Tsigkourakos, Menelaos; Sasso, Luigi; Buijnsters, Josephus G.

DOI
10.1016/j.diamond.2019.03.017

Publication date
2019

Document Version
Final published version

Published in
Diamond and Related Materials

Diamond & Related Materials 95 (2019) 20–27

Contents lists available at ScienceDirect

Diamond & Related Materials

journal homepage: www.elsevier.com/locate/diamond

Template-assisted bottom-up growth of nanocrystalline diamond micropillar arrays☆

André F. Sartori*, Bart H.L. Overes, Paola Fanzio, Menelaos Tsigkourakos[1], Luigi Sasso, Josephus G. Buijnsters*

Department of Precision and Microsystems Engineering, Research Group of Micro and Nano Engineering, Delft University of Technology, Mekelweg 2, 2628 CD Delft, The Netherlands

ARTICLE INFO

Keywords:
Bottom-up growth
Micropillar arrays
CVD diamond
Imprint lithography
Template

ABSTRACT

Micro-patterned diamond has been investigated for numerous applications, such as biomimetic surfaces, electrodes for cell stimulation and energy storage, photonic structures, imprint lithography, and others. Controlled patterning of diamond substrates and moulds typically requires lithography-based top-down processing, which is costly and complex. In this work, we introduce an alternative, cleanroom-free approach consisting of the bottom-up growth of nanocrystalline diamond (NCD) micropillar arrays by chemical vapour deposition (CVD) using a commercial porous Si membrane as a template. Conformal pillars of ~4.7 μm in height and ~2.2 μm in width were achieved after a maximum growth time of 9 h by hot-filament CVD (2% CH_4 in H_2, 725 °C at 10 mbar). In order to demonstrate one of many possible applications, micropillar arrays grown for 6 h, with ~2 μm in height, were evaluated as moulds for imprint lithography by replication onto hard cyclic olefin copolymer (COC) and onto soft polydimethylsiloxane (PDMS) elastomer. The results showed preserved mechanical integrity of the diamond moulds after replication, as well as full pattern transfer onto the two polymers, with matching dimensions between the grown pillars and the replicated holes. Prior surface treatment of the diamond mould was not required for releasing the PDMS replica, whereas the functionalisation of the diamond surface with a perfluorododecyltrichlorosilane (FDDTS) anti-stiction layer was necessary for the successful release of the COC replica from the mould. In summary, this paper presents an alternative and facile route for the fabrication of diamond micropillar arrays and functional micro-textured surfaces.

1. Introduction

Diamond is a material with desirable mechanical and chemical properties for biomimetic structures [1–3], (bio)electrochemistry [4], imprint lithography [5] and other applications, due to its high Young's modulus (up to ~10^6 N mm^{-2}), high thermal conductivity (> 2000 W m^{-1} K^{-1}) [4], low thermal expansion coefficient (10^{-6} K^{-1} at 300 K) [6], low coefficient of friction [7], non-toxicity, and versatile surface chemistry. Many of those applications require patterning of the diamond surface into regular functional structures, such as nanowires [8,9], micro/nanopillars, microchannels [10] and pads [11], which are normally achieved by multistep lithography (photo-, e-beam, focused ion beam) and/or etching processes [12,13]. For this reason, new fabrication routes aimed at reducing complexity and cost have been increasingly investigated. These include, for example, the formation of periodic surface structures by laser for the creation of photonic structures [14] and enhanced electrodes [15], the combination of diamond with foreign scaffold materials to enhance the surface area in electrode [16], biosensing [17] and field-emission [18] applications, the selective seeding of diamond nanoparticles through micropipetting [19], inkjet printing [20,21] and surface functionalisation [22], and the use of porous alumina templates [23,24] for the bottom-up growth of diamond micro/nanostructures.

The latter approach is attractive, since it shifts the need for patterning to materials which are easier to process and which enjoy a more mature and well-established industry. An obvious material candidate for that purpose is anodised aluminium oxide (AAO), which has been previously applied as etching masks for the fabrication of porous diamond membranes [23], as well as a template for growth of diamond nanopillars [24]. However, the pore size of AAO is limited to the sub-

☆ The authors declare no competing financial interest.

* Corresponding authors.
E-mail addresses: A.FrotaSartori@tudelft.nl (A.F. Sartori), J.G.Buijnsters@tudelft.nl (J.G. Buijnsters).
[1] Present address: Department of Applied Physics, National Technical University of Athens, Iroon Polytechniou 9, 15780 Athens, Greece.

https://doi.org/10.1016/j.diamond.2019.03.017
Received 8 February 2019; Received in revised form 25 March 2019; Accepted 25 March 2019
Available online 26 March 2019

micrometre range, the pore distribution lacks long-range order, and the membranes can be an undesired source of contaminants, such as Al and chemical residuals from the anodising process, into the chemical vapour deposition (CVD) chamber. Silicon, on the other hand, can be micropatterned on an industrial scale and does not have the drawbacks of AAO. For those reasons, we devoted this work to the study of bottom-up growth of diamond micropillars utilising commercially available, pre-patterned silicon templates. The resulting diamond microstructures were employed as moulds for imprint lithography to demonstrate one of many possible applications.

Micro-/nanoimprint lithography is a high-throughput, high-resolution, and low-cost contact patterning method used to create microfluidic devices and optical components, and to overcome resolution limits with photolithography [25]. The surface pattern of a mould is replicated onto a thermoplastic material or onto a resist by mechanical contact and three-dimensional material displacement. The moulds can be exposed to elevated pressures and temperatures and need to be used repeatedly and reproducibly. Diamond is an attractive material for imprint lithography moulds, due to its high hardness, high thermal conductivity, low thermal expansion coefficient, chemical inertness and wear resistance. Up until now, diamond stamps were fabricated using single crystal or polished CVD diamond, which are micro-structured by focused ion beam, reactive ion etching or e-beam lithography, where scalability and cost are an issue [5,26–28]. Thus, template-based bottom-up growth of diamond microstructures may enable the production of diamond moulds on wafer scale and help bring costs down.

In this work, we show the steps towards the successful fabrication of nanocrystalline diamond micro-pillar arrays on silicon and their replication onto two different polymers: cyclic olefin copolymer (COC) developed by TOPAS®, and polydimethylsiloxane (PDMS), which are important materials for the fabrication of microfluidic, lab-on-chip and biosensing devices [29,30]. The mould replication onto COC was performed by hot-embossing at high pressure and temperature, while the replication onto PDMS was carried out at ambient conditions. The pattern transfer was analysed by a combination of 3D optical profilometry and scanning electron microscopy (SEM).

2. Experimental

2.1. Diamond micropillar growth

Fig. 1 illustrates the fabrication steps of the diamond micropillar master mould. In a first step, 1) a ~1.5 × 1.5 cm^2 piece of bare silicon wafer of 0.4 mm thickness (with native oxide) was spin-seeded with detonation nanodiamond particles, according to the procedure described elsewhere [31]. Then, 2) the seeded wafer was loaded into a home-built hot-filament chemical vapour deposition (HFCVD) chamber for the growth of a thin layer of nanocrystalline diamond (NCD) of ~0.2 µm thickness for 15 min, performed at our standard conditions: 725 °C, 10 mbar, with 6 sccm CH_4 and 300 sccm H_2. Subsequently, 3) a porous Si membrane (1 × 1 cm^2, ~17 µm thick, with square ~2.5 × 2.5 $µm^2$ pores arranged in a hexagonal pattern with ~4.2 µm pitch) from SmartMembranes GmbH, Germany, was placed onto the grown NCD layer, and supported at the corners with additional pieces of Si. 4) The Si/NCD/membrane wafer was then loaded into the HFCVD chamber for further growth for up to 9 h. After that, 5) the membrane was mechanically and chemically removed, in order to expose the newly formed diamond micropillars. For short growth duration, before mechanical interlocking between the pillars and the membrane holes occurs, ultrasonication in acetone was sufficient to remove the membrane. For longer growth duration, when the pillars are interlocked with the membrane, only parts of the membrane can be pulled off mechanically (*e.g.* with a tweezer). The chemical process was thus necessary to etch away the remaining pieces of the membrane, and consisted of dipping the sample in a bath of concentrated, boiling KOH, for a few minutes, until the membrane had been removed completely. The process was completed with cleaning in a boiling concentrated mixture of HCl + H_2SO_4 + HNO_3, which removed remaining carbon deposits and promoted the oxygenation of the diamond surface as a side-effect. The samples were rinsed in deionised water as a final step.

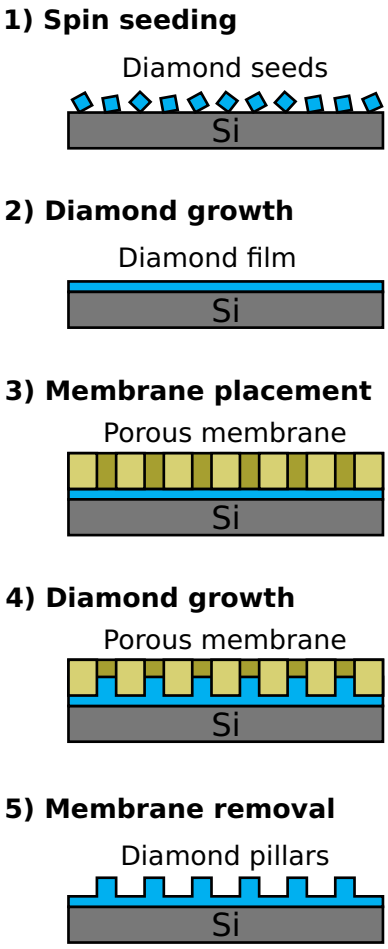

Fig. 1. Fabrication steps of the diamond micropillar master mould.

2.2. Mould replication onto COC and PDMS

Fig. 2 illustrates the replica moulding procedures. Replication into polydimethylsiloxane (PDMS) was achieved by casting a PDMS solution (10 parts of elastomer to 1 part curing agent, w/w ratio) onto the diamond master mould and letting it cure at 70–80 °C for at least 1 h. After that, the PDMS replica was peeled off from the diamond mould and further analysed. Mould replication onto cyclic olefin copolymer (COC) was achieved by hot-embossing the diamond micropillar master mould onto a 1 mm thick COC wafer, grade 6013 from TOPAS®, in an EVG510 wafer bonder setup equipped for the purpose. The procedure was performed in vacuum, with a load of ~2500 N applied for 8 min, at 170 °C (above the COC's glass transition temperature of 130 °C). After this time, the sample was let cool down to room temperature, still under load, and released thereafter. The COC was manually demoulded. In order to facilitate the latter step and avoid breaking the thin silicon wafer, the diamond micropillar master mould was previously coated with a FDDTS anti-stiction layer, as described below.

2.3. 1H, 1H, 2H, 2H-Perfluorododecyltrichlorosilane (FDDTS) anti-stiction layer

The diamond micropillar master moulds were coated with FDDTS before hot-embossing into COC. The acid cleaning treatment described

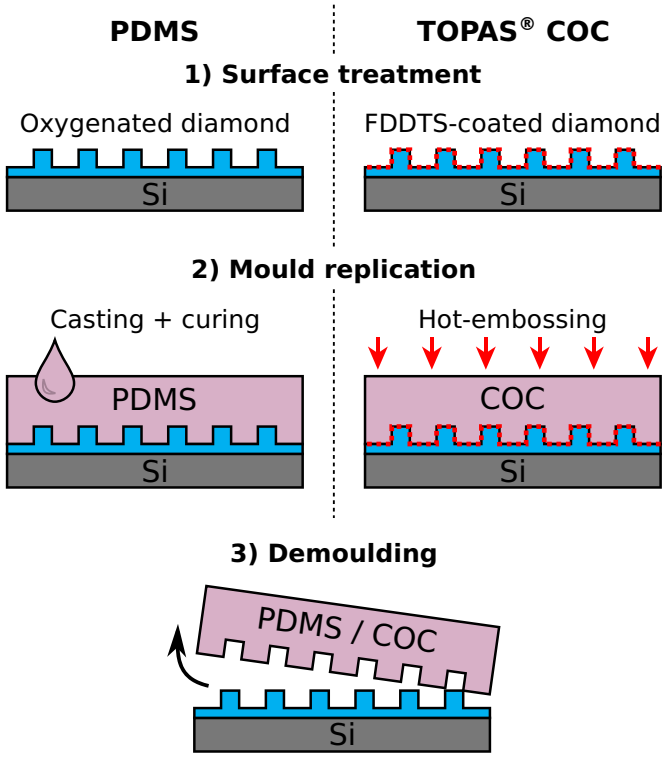

Fig. 2. Fabrication steps of the PDMS and COC mould replicas.

earlier produced the necessary oxygenation of the diamond surface for the binding of the FDDTS molecules. 1H, 1H, 2H, 2H-Perfluorododecyltrichlorosilane (97% purity) was obtained from Sigma-Aldrich, and diluted in ethanol (1% w/w ratio). The moulds were dipped into the solution and ultrasonicated for 30 s, then left resting for 30 min. After that, the moulds were taken out and ultrasonicated in ethanol for 30 s, followed by baking at ~130 °C on a hot plate for 30 min.

2.4. Structure and morphology characterisation

Scanning electron microscopy (SEM) measurements were performed with a JEOL JSM-6010LA scanning electron microscope, at 5 keV and secondary electron detector, and with a field-emission FEI Nova NanoSEM 450 setup operating at 15 keV, with a high-resolution (immersion mode) secondary electron detector. Raman spectroscopy measurements were performed with a Horiba LabRAM HR setup, equipped with an argon ion laser operating at 514 nm, and spectral resolution of ~0.3 cm^{-1}. Height profile imaging of the patterned samples was performed with a Bruker Contour GT-K 3D optical profilometer operating at highest (100×) magnification, with white light illumination, and VXI mode for best accuracy.

3. Results and discussion

3.1. Template characterisation

Fig. 3 shows SEM micrographs of the porous silicon membrane used as a template for the growth of diamond micropillars. Apart from confirming the dimensions specified by the supplier (see Section 2.1 above), notable characteristics of the template were the bottleneck at about ~1 μm depth into the pores, which is ~1.8 μm wide, whereas the overall pore diameter reaches up to 2.5 μm. Fig. 3(c) shows how the square pores morph into a more rounded shape along the depth of the membrane.

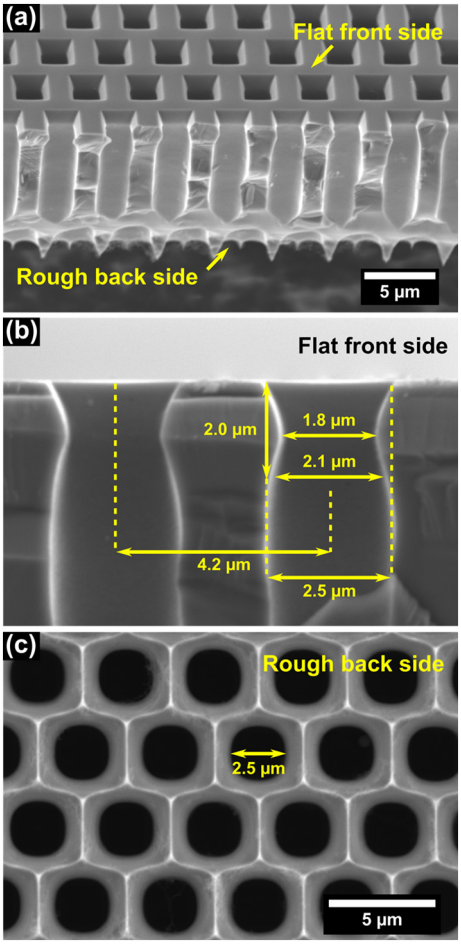

Fig. 3. SEM micrographs of the porous silicon membrane from SmartMembranes GmbH used to synthesise the NCD micropillars. (a) Tilted surface. (b) Cross section. The flat front side faced the initial NCD layer for the micropillar growth. (c) Backside. The nominal dimensions are: membrane size of 1 × 1 cm^2, ~17 μm thickness, pore diameter of up to ~2.5 μm and centroid distance (pitch) of ~4.2 μm.

3.2. Diamond micropillars

Several diamond micropillar samples were produced, with different growth durations from 3 to 9 h. Before placing the Si template, a ~0.2 μm thick NCD layer was grown in order to ensure a closed diamond film at the bottom. The template was then placed onto it, with the flat front side facing down, and the diamond growth was resumed. After removing the template, the produced samples were imaged by SEM (Fig. 4(a–c)) and analysed by Raman spectroscopy (Fig. 4(d)). The SEM images show that diamond grows selectively into the pores of the template, leading to very well-defined, uniform and well-aligned microstructures. As expected from the pore shape, the pillars evolved from squares to rounded squares, and are narrow near the base, matching the bottleneck inside the pores of the template shown in Fig. 3(b). Fig. 4(e) shows an optical microscopy image of the sample surface with NCD micropillars grown for 9 h. The iridescent area at the centre corresponds to two growth zones (as indicated by the numbers): (1) fully grown pillars and (2) pillar height gradient. Outside the iridescent area, in zone (3), the NCD layer grew flat. The reason for this variation is explained in Fig. 5 below. The Raman spectrum of a random micropillar after 6 h growth is compared in Fig. 4(d) with the spectrum measured outside the template area (*i.e.* flat NCD layer), as indicated by the inset SEM images. The combination of the well-known diamond one-phonon line at 1333 cm^{-1} [32] with prominent D- and G-bands confirms that

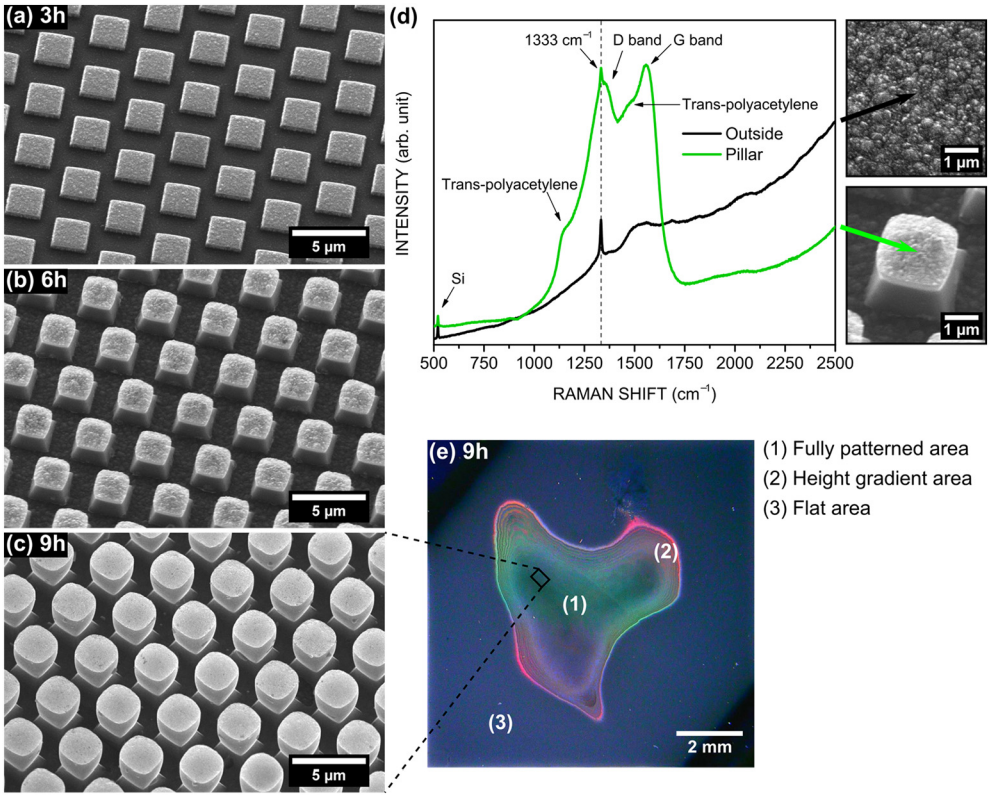

Fig. 4. (a–c) SEM micrographs of the template-grown NCD micropillars after growth for (a) 3 h, (b) 6 h and (c) 9 h. Note how the bottleneck inside the pores of the template (Fig. 3(b)) shaped the base of the diamond pillars after 6 h. (d) Raman spectra (as-measured) taken from the top of the micropillar (green curve) and from outside the membrane/patterned area (black curve) for comparison. (e) Optical microscopy image of the 9 h sample, showing distinct growth zones indicated by the numbers (1–3). The complete image corresponds to the $1 \times 1\ cm^2$ area which was covered by the Si template. The dark areas at the upper-left and bottom-right corners match the location of the supporting Si pieces used to hold the membrane in place during the growth process.

the material on the pillar is diamond, with a high percentage of sp^2 carbon [33–35]. The flat NCD film grown freely outside the membrane shows relatively lower sp^2 carbon content, as seen from the less intense G-band and virtually absent D-band. The observed difference is due to the change in local growth environment around the template pores, which, on the one hand, partially inhibit the growth species (atomic hydrogen and C_xH_y radicals) from reaching the diamond surface, thus decreasing the local growth rate, and, on the other hand, likely serve as a local source of carbon from deposits on the membrane. The overall effect on the composition is comparable to growing NCD with higher $[CH_4]/[H_2]$ ratio. In addition to the overall shape, the Raman spectrum on the pillar also shows the presence of peaks related to *trans*-polyacetylene, which are common signatures in nanocrystalline diamond [35,36]. The silicon peak at 520.7 cm^{-1} arises from the underlying Si substrate. Overall, the SEM and Raman results show that the NCD material grew homogeneously and conformally into the pores.

Fig. 5 illustrates the development of the NCD micropillars through the template pores as a function of time, but also as a function of the gap between the Si template and the NCD substrate. The left column (zero gap) corresponds to the fully patterned growth zone where the micropillars started to grow immediately from the beginning of the CVD growth process, which is the situation shown in Fig. 4(a–c),

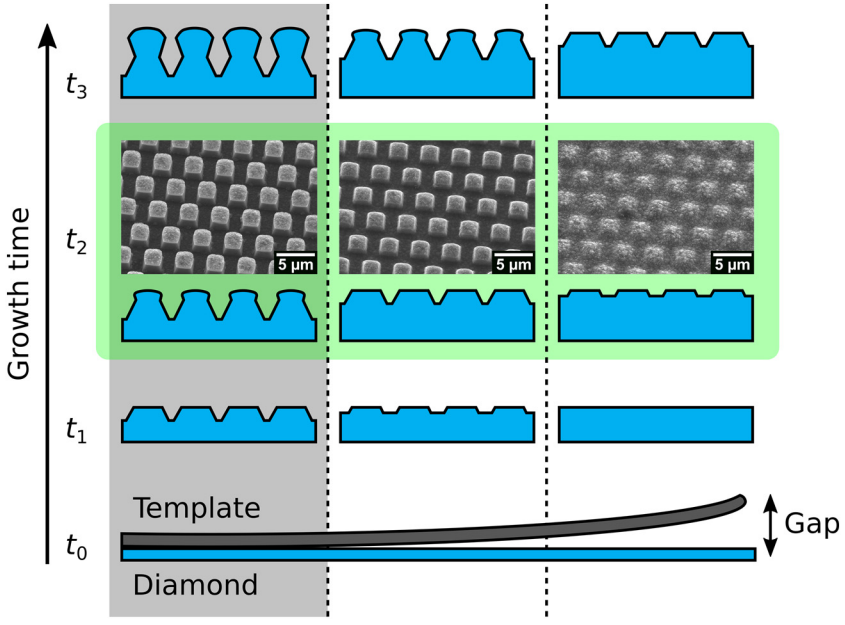

Fig. 5. Illustration of how the NCD micropillars develop during growth through the template pores as a function of growth time (vertical direction) and the gap between the pre-grown flat NCD layer and the Si template (horizontal direction). The zero-gap column on the left (shaded grey background) corresponds to the samples shown in Fig. 4(a–c), with $t_1 = 3$ h, $t_2 = 6$ h and $t_3 = 9$ h. The t_2 line shows how the pillar height decreases with increasing template gap on the 6 h sample.

respectively for $t_1 = 3$ h, $t_2 = 6$ h and $t_3 = 9$ h. Fig. 5 also shows SEM images of the 6 h sample as a function of template gap in the t_2 row. As the template gap increases due to buckling, because the Si membrane is very thin (~17 μm), the additional time it takes for the underlying NCD layer to reach the base of the template before NCD pillars can develop through the pores, leads to smaller pillar height. In the extreme case where the gap is too large for duration of the NCD growth process, the diamond remains flat in that zone. The resulting optical effect of such variations on the NCD micropillar formation is shown in Fig. 4(e) for the 9 h sample, as described earlier.

3.3. COC replica

After growth for 6 h, the diamond micropillar master mould was coated with a FDDTS anti-stiction layer, and then hot-embossed into COC (negative replica). After cooling down to near room temperature, the replica was mechanically detached from the diamond master mould and used as a mould for replication onto PDMS (positive replica), in order to reproduce the shape of the diamond micropillars from the COC replica. The three samples (*i.e.*, the diamond master mould and the two polymer replicas) were analysed by 3D optical profilometry, as shown in Fig. 6(a–c). SEM images of the COC and PDMS replicas are shown in Fig. 7(a,b), respectively. It can be seen in Fig. 6(a–c) that the diamond micropillars resulted homogeneous in both lateral and vertical dimensions, whereas the COC replica resulted in a somewhat less regular pattern, with slight distortion of the hole perimeter. Extra irregularities on the top surface can also be seen. On the other hand, the PDMS replica shows pillars matching the original diamond master mould very closely in both lateral and vertical dimensions. Vertical and horizontal line profiles of the three areas (taken along the indicated dashed lines) are compared in Fig. 6(d). They show a clear match between the pillars and the holes, and a full imprint into the ~2 μm inter-pillar depth. A statistical distribution obtained from particle analysis of the three top-view images is given in Fig. 6(e). The results are summarised in Table 1. The area corresponds to either the top surface of the pillars or the bottom surface of the holes.

The statistical analysis of the optical profilometry images shows a mismatch between the area of the top of the pillars of the diamond master mould and that of the bottom of the holes in the COC negative replica, with the holes in the COC ~24% smaller than the pillars on the mould, and with ~2.2% smaller nearest neighbour distance. Considering that the COC cooled down from 170 °C (above its glass transition temperature) to 25 °C, and taking into account its thermal expansion coefficient, $\varepsilon_{COC} = 0.6 \times 10^{-4} K^{-1}$, the expected contraction purely due to thermal expansion is only 0.90%. Thus, although this may have contributed to the observed 2.2% shrinkage in length, thermal shrinkage alone cannot explain the relatively smaller size of the holes. The statistical analysis shows, however, a very good match between the PDMS positive replica and the diamond master mould, with matching dimensions between pillars and holes, and retained average nearest neighbour distance from the COC. This suggests that the area of the COC holes measured by optical profilometry was underestimated, mostly likely due to optical artefacts at the edges of the structures from the limited lateral resolution of the setup. This is confirmed by the SEM image of the COC, shown in Fig. 7(a), where the hole dimensions match those of the original mould. Thus, overall, the replication of the diamond master mould onto COC was successful.

3.4. PDMS replica

After growth for 6 h, a diamond micropillar master mould was replicated onto PDMS as illustrated in Fig. 2, resulting in an imprinted structure similar to the COC replica discussed above, as shown in Fig. 8(a,b). Fig. 8(c) compares the line profiles of the two samples in

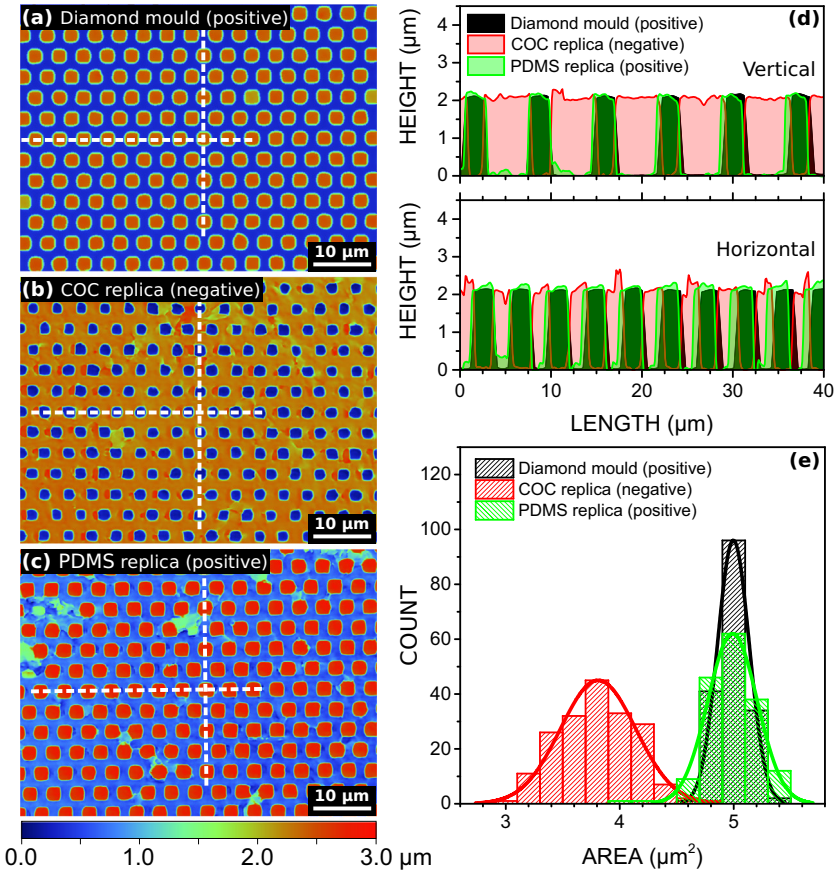

Fig. 6. (a–c) 3D optical profilometry image of (a) the 6 h diamond master mould, (b) the COC replica, and (c) the PDMS replica of the COC replica. (d) Comparison of the vertical and horizontal line profiles, taken from (a), (b) and (c) as indicated by the white dashed lines. (e) Histogram ($n = 33$) of the area of the top of pillars from (a,c) and of the bottom of the holes from (b).

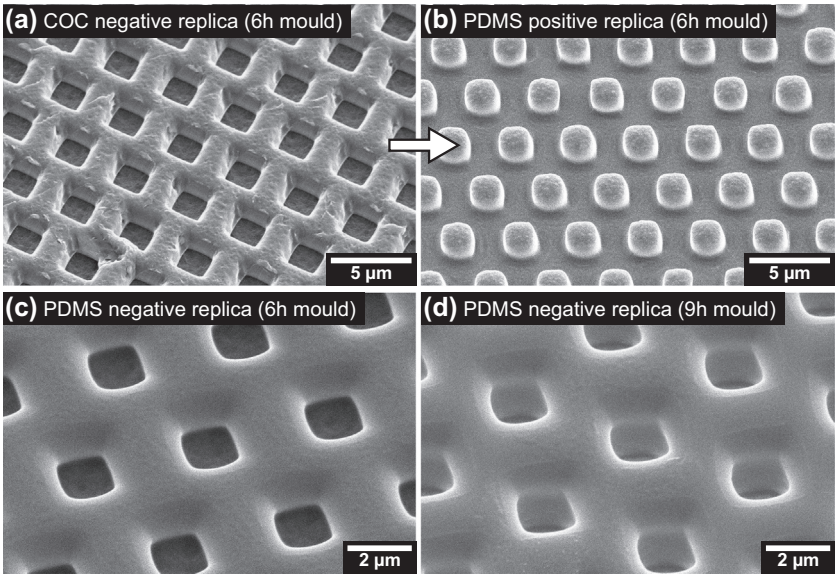

Fig. 7. Tilted (30°) SEM micrographs of (a) the COC negative replica shown in Fig. 6(b), (b) the PDMS positive replica (see Fig. 6(c)) of the COC replica shown in (a), (c,d) PDMS negative replicas of the diamond master moulds grown for (c) 6 h and (d) 9 h, respectively. The yellow outlines in (c) and (d) are a guide for the eye to highlight the difference in pore depth between the two samples. (For interpretation of the references to color in this figure legend, the reader is referred to the web version of this article.)

Table 1
Summary of the statistical analysis of the 3D optical profilometry images shown in Fig. 6. The given numbers are average values ± standard deviation (σ).

Sample	Area ± σ (µm^2)	Square length ± σ (µm)	Nearest neighbour distance ± σ (µm)
Diamond master mould, 6 h	5.00 ± 0.14	2.24 ± 0.03	4.11 ± 0.02
COC (negative) replica	3.81 ± 0.33	1.95 ± 0.03	4.02 ± 0.06
PDMS (positive) replica	4.99 ± 0.22	2.23 ± 0.05	4.02 ± 0.04

both vertical and horizontal directions, as indicated by the dashed lines in Fig. 8(a,b). Fig. 8(d) shows histograms of the areas of both the pillars and the holes, derived from statistical analysis of the 3D optical profilometry images. The results are given in Table 2, and show full replication of the mould onto the PDMS, with similar height/depth and lateral dimensions between the pillars and the holes. Nearest neighbour analysis resulted in ~1% contraction of the PDMS replica, relative to the diamond mould, which explains the minor offset seen between the

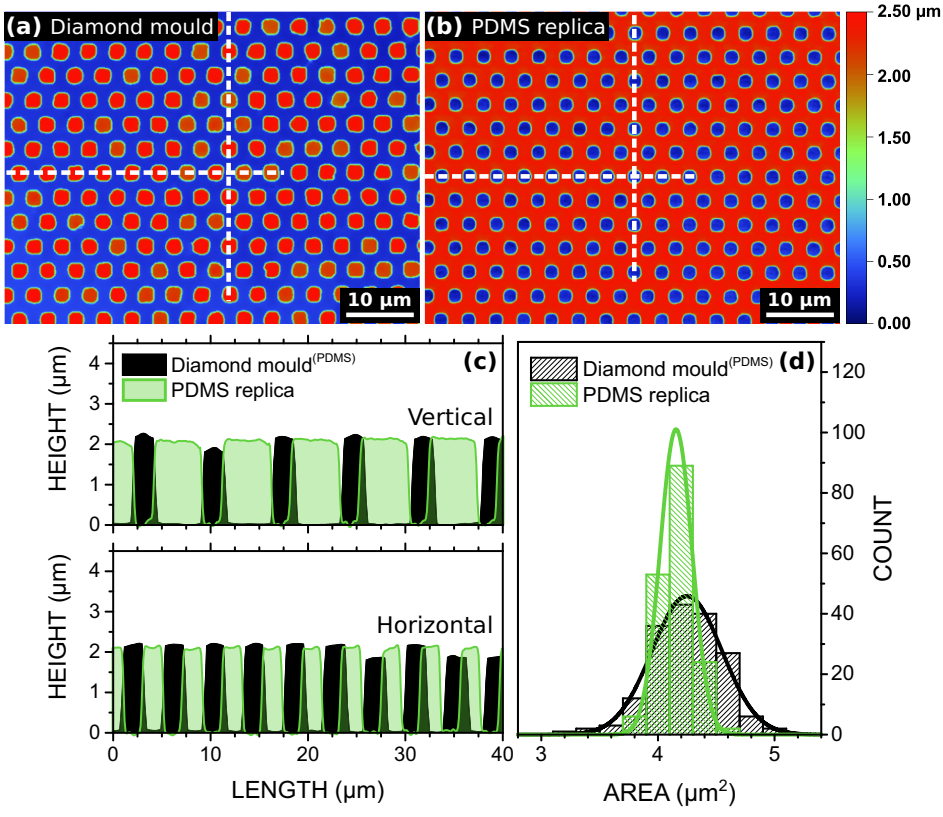

Fig. 8. (a,b) 3D optical profilometry image of (a) the 6 h diamond mould and of (b) its PDMS replica. (c) Comparison of the vertical and horizontal line profiles, taken from (a) and (b) as indicated by the white dashed lines. (d) Histogram (n = 25) of the area of the top of pillars from (a) and of the bottom of the imprinted holes from (b).

Table 2
Summary of the statistical analysis of the 3D optical profilometry images shown in Fig. 8. The given numbers are average values ± standard deviation (σ).

Sample	Area ± σ (μm^2)	Square length ± σ (μm)	Nearest neighbour distance ± σ (μm)
Diamond mould, 6 h	4.26 ± 0.29	2.06 ± 0.07	4.08 ± 0.04
PDMS (negative) replica	4.16 ± 0.14	2.04 ± 0.03	4.04 ± 0.02

line scans shown in Fig. 8(c). The SEM image of the PDMS replica in Fig. 7(c) resembles that of the original Si template (Fig. 3(a)) with its distinct trapezoidal profile until the bottleneck, albeit smoothed. The results show that, like for COC, the diamond mould was fully replicated into the PDMS, with the resulting holes displaying matching depth to the pillar height.

For comparison, the 9 h diamond micropillar master mould shown in Fig. 4(c) was also replicated onto PDMS, resulting in the structure shown in Fig. 7(d). It can be seen that the replica is very similar to the replica of the 6 h mould (Fig. 7(c)), but with deeper holes, as highlighted by the yellow outlines. The compliance of the PDMS made its release from the 9 h mould possible, despite the bottleneck shape of the micropillars. Such approach was not feasible with COC, as a result of the higher stiffness of the copolymer material.

In summary, the results show that bottom-up fabrication of NCD micropillars can be achieved with the use of commercial porous Si membranes as growth templates, with potential use as biomimetic devices, enhanced electrodes, or moulds for imprint lithography. The latter was demonstrated above, with the successful application of the NCD micropillars for imprint lithography onto COC and PDMS.

4. Conclusion

In this work, we demonstrated the bottom-up growth of nanocrystalline diamond micropillars by chemical vapour deposition using a microporous Si template mask. Conformal NCD pillars were grown inside the ~2.2 μm square pores up to a height of ~4.7 μm for 9 h growth. The NCD micro-pillars grown for 6 h (~2 μm in height) were applied as moulds for imprint lithography on COC (hard polymer) and PDMS (soft polymer), resulting in full mould replication in both cases. Replication of taller pillars into COC was limited due to mechanical interlocking caused by the bottleneck shape of the pillars, which was inherited from the commercial Si membrane. For smaller pillars, replication onto COC was only possible with the addition of a fluorine-based anti-stiction layer, whereas for replication onto PDMS no additional surface treatment was necessary. The presented template-assisted method for the growth of NCD microstructures may find important applications in diamond-based biomimetic and photonic devices, enhanced (bio)electrodes, as well as moulds for imprint lithography.

Acknowledgements

The authors thank the PME technical team for the lab support.

References

[1] R. Manai, E. Scorsone, L. Rousseau, F. Ghassemi, M. Possas Abreu, G. Lissorgues, N. Tremillon, H. Ginisty, J.C. Arnault, E. Tuccori, M. Bernabei, K. Cali, K.C. Persaud, P. Bergonzo, Grafting odorant binding proteins on diamond bio-MEMS, Biosens. Bioelectron. 60 (2014) 311–317, https://doi.org/10.1016/j.bios.2014.04.020.
[2] E. Granados, M.M. Calderon, J. Krzywinski, E. Wörner, A. Rodriguez, M.G. Aranzadi, S.M. Olaizola, Enhancement of surface area and wettability properties of boron doped diamond by femtosecond laser-induced periodic surface structuring, Opt. Mater. Express. 7 (2017) 3389–3396, https://doi.org/10.1364/OME.7.003389.
[3] Z. Tian, W. Huang, B. Xu, X. Li, Y. Mei, Anisotropic rolling and controlled chirality of nanocrystalline diamond nanomembranes toward biomimetic helical frameworks, Nano Lett. 18 (2018) 3688–3694, https://doi.org/10.1021/acs.nanolett.8b00828.
[4] S. Szunerits, C.E. Nebel, R.J. Hamers, Surface functionalization and biological applications of CVD diamond, MRS Bull. 39 (2014) 517–524, https://doi.org/10.1557/mrs.2014.99.
[5] J. Taniguchi, Y. Tokano, I. Miyamoto, M. Komuro, H. Hiroshima, K. Kobayashi, T. Miyazaki, H. Ohyi, Preparation of diamond mold using electron beam lithography for application to nanoimprint lithography, Jpn. J. Appl. Phys. 39 (2000) 7070–7074, https://doi.org/10.1143/JJAP.39.7070.
[6] S. Stoupin, Y. V Shvyd'ko, Ultraprecise studies of the thermal expansion coefficient of diamond using backscattering x-ray diffraction, Phys. Rev. B. 83 (2011) 104102.
[7] J.G. Buijnsters, M. Tsigkourakos, T. Hantschel, F.O.V. Gomes, T. Nuytten, P. Favia, H. Bender, K. Arstila, J.-P. Celis, W. Vandervorst, Effect of boron doping on the wear behavior of the growth and nucleation surfaces of micro- and nanocrystalline diamond films, ACS Appl. Mater. Interfaces 8 (2016) 26381–26391, https://doi.org/10.1021/acsami.6b08083.
[8] S. Szunerits, Y. Coffinier, E. Galopin, J. Brenner, R. Boukherroub, Preparation of boron-doped diamond nanowires and their application for sensitive electrochemical detection of tryptophan, Electrochem. Commun. 12 (2010) 438–441, https://doi.org/10.1016/j.elecom.2010.01.014.
[9] P.W. May, M. Clegg, T.A. Silva, H. Zanin, O. Fatibello-Filho, V. Celorrio, D.J. Fermin, C.C. Welch, G. Hazell, L. Fisher, A. Nobbs, B. Su, Diamond-coated "black silicon" as a promising material for high-surface-area electrochemical electrodes and antibacterial surfaces, J. Mater. Chem. B 4 (2016) 5737–5746, https://doi.org/10.1039/C6TB01774F.
[10] A. Karczemska, Diamond materials for microfluidic devices, in: Diamond-based Mater, Woodhead Publishing, Biomed. Appl, 2013, pp. 256–271, https://doi.org/10.1533/9780857093516.2.256.
[11] R. Ramaneti, K.J. Sankaran, S. Korneychuk, C.J. Yeh, G. Degutis, K.C. Leou, J. Verbeeck, M.K. Van Bael, I.N. Lin, K. Haenen, Vertically aligned diamond-graphite hybrid nanorod arrays with superior field electron emission properties, APL Mater. 5 (6) (2017) 066102, , https://doi.org/10.1063/1.4985107.
[12] P.A. Nistor, P.W. May, Diamond thin films: giving biomedical applications a new shine, J. R. Soc. Interface 14 (2017), https://doi.org/10.1098/rsif.2017.0382.
[13] S. Castelletto, L. Rosa, J. Blackledge, M.Z. Al Abri, A. Boretti, Advances in diamond nanofabrication for ultrasensitive devices, Microsystems Nanoeng. 3 (2017) 17061, https://doi.org/10.1038/micronano.2017.61.
[14] E. Granados, M. Martinez-Calderon, M. Gomez, A. Rodriguez, S.M. Olaizola, Photonic structures in diamond based on femtosecond UV laser induced periodic surface structuring (LIPSS), Opt. Express 25 (2017) 15330–15335, https://doi.org/10.1364/OE.25.015330.
[15] A.F. Sartori, S. Orlando, A. Bellucci, D.M. Trucchi, S. Abrahami, T. Boehme, T. Hantschel, W. Vandervorst, J.G. Buijnsters, Laser-Induced Periodic Surface Structures (LIPSS) on heavily boron-doped diamond for electrode applications, ACS Appl. Mater. Interfaces 10 (2018) 43236–43251, https://doi.org/10.1021/acsami.8b15951.
[16] F. Gao, C.E. Nebel, Diamond-based supercapacitors: realization and properties, ACS Appl. Mater. Interfaces 8 (2016) 28244–28254, https://doi.org/10.1021/acsami.5b07027.
[17] G. Piret, C. Hébert, J.-P. Mazellier, L. Rousseau, E. Scorsone, M. Cottance, G. Lissorgues, M.O. Heuschkel, S. Picaud, P. Bergonzo, B. Yvert, 3D-nanostructured boron-doped diamond for microelectrode array neural interfacing, Biomaterials. 53 (2015) 173–183, https://doi.org/10.1016/j.biomaterials.2015.02.021.
[18] Y. Zou, P.W. May, S.M.C. Vieira, N.A. Fox, Field emission from diamond-coated multiwalled carbon nanotube "teepee" structures, J. Appl. Phys. 112 (2012) 044903, , https://doi.org/10.1063/1.4748336.
[19] A.C. Taylor, R. Edgington, R.B. Jackman, Patterning of nanodiamond tracks and nanocrystalline diamond films using a micropipette for additive direct-write processing, ACS Appl. Mater. Interfaces 7 (2015) 6490–6495, https://doi.org/10.1021/am507900a.
[20] N.A. Fox, M.J. Youh, J.W. Steeds, W.N. Wang, Patterned diamond particle films, J. Appl. Phys. 87 (2000) 8187–8191, https://doi.org/10.1063/1.373516.
[21] A.F. Sartori, P. Belardinelli, R.J. Dolleman, P.G. Steeneken, M.K. Ghatkesar, J.G. Buijnsters, Inkjet-printed high- Q nanocrystalline diamond resonators, Small. 15 (2019) 1803774, https://doi.org/10.1002/smll.201803774.
[22] P. Pobedinskas, G. Degutis, W. Dexters, W. Janssen, S.D. Janssens, B. Conings, B. Ruttens, J. D'Haen, H.-G. Boyen, A. Hardy, M.K. Van Bael, K. Haenen, Surface plasma pretreatment for enhanced diamond nucleation on AlN, Appl. Phys. Lett. 102 (2013) 201609, https://doi.org/10.1063/1.4807591.
[23] H. Masuda, M. Watanabe, K. Yasui, D. Tryk, T. Rao, A. Fujishima, Fabrication of a nanostructured diamond honeycomb film, Adv. Mater. 12 (2000) 444–447, https://doi.org/10.1002/(SICI)1521-4095(200003)12:6<444::AID-ADMA444>3.0.CO;2-K.
[24] H. Masuda, T. Yanagishita, K. Yasui, K. Nishio, I. Yagi, T.N. Rao, A. Fujishima, Synthesis of well-aligned diamond nanocylinders, Adv. Mater. 13 (2001) 247–249, https://doi.org/10.1002/1521-4095(200102)13:4<247::AID-ADMA247>3.0.CO;2-H.
[25] M.C. Traub, W. Longsine, V.N. Truskett, Advances in nanoimprint lithography, Annu. Rev. Chem. Biomol. Eng. 7 (2016) 583–604, https://doi.org/10.1146/annurev-chembioeng-080615-034635.
[26] J. Taniguchi, Y. Tokano, I. Miyamoto, M. Komuro, H. Hiroshima, Diamond

nanoimprint lithography, Nanotechnology. 13 (2002) 592–596, https://doi.org/10.1088/0957-4484/13/5/309.
[27] Y. Hirai, S. Yoshida, N. Takagi, Y. Tanaka, H. Yabe, K. Sasaki, H. Sumitani, K. Yamamoto, High aspect pattern fabrication by nano imprint lithography using fine diamond Mold, Jpn. J. Appl. Phys. 42 (2003) 3863–3866, https://doi.org/10.1143/JJAP.42.3863.
[28] M. Komori, H. Uchiyama, H. Takebe, T. Kusuura, K. Kobayashi, H. Kuwahara, T. Tsuchiya, Micro/nanoimprinting of glass under high temperature using a CVD diamond mold, J. Micromechanics Microengineering. 18 (2008) 65013, https://doi.org/10.1088/0960-1317/18/6/065013.
[29] P. Fanzio, A. Cagliani, K.G. Peterffy, L. Sasso, High throughput soft embossing process for micro-patterning of PEDOT thin films, Microelectron. Eng. 176 (2017) 15–21, https://doi.org/10.1016/j.mee.2017.01.011.
[30] P. Fanzio, C.-T. Chang, M. Skolimowski, S. Tanzi, L. Sasso, Fully-polymeric pH sensor realized by means of a single-step soft embossing technique, Sensors. 17 (2017) 1169, https://doi.org/10.3390/s17051169.
[31] M. Tsigkourakos, T. Hantschel, S.D. Janssens, K. Haenen, W. Vandervorst, Spin-seeding approach for diamond growth on large area silicon-wafer substrates, Phys. Status Solidi 209 (2012) 1659–1663, https://doi.org/10.1002/pssa.201200137.
[32] C. Ramaswamy, Raman effect in diamond, Nature. 125 (1930) 704, https://doi.org/10.1038/125704b0.
[33] A. Merlen, J.G. Buijnsters, C. Pardanaud, A guide to and review of the use of multiwavelength Raman spectroscopy for characterizing defective aromatic carbon solids: from graphene to amorphous carbons, Coatings. 7 (2017) 153, https://doi.org/10.3390/coatings7100153.
[34] S. Prawer, R.J. Nemanich, Raman spectroscopy of diamond and doped diamond, Philos. Trans. R. Soc. London A Math. Phys. Eng. Sci. 362 (2004) 2537–2565, https://doi.org/10.1098/rsta.2004.1451.
[35] F. Andrea Carlo, J. Robertson, Raman spectroscopy of amorphous, nanostructured, diamond-like carbon, and nanodiamond, Philos. Trans. Math. Phys. Eng. Sci. 362 (2004) 2477–2512, https://doi.org/10.1098/rsta.2004.1452.
[36] J.G. Buijnsters, L. Vázquez, Growth dynamics of nanocrystalline diamond thin films deposited by hot filament chemical vapor deposition: influence of low sticking and renucleation processes, J. Phys. Chem. C 115 (2011) 9681–9691, https://doi.org/10.1021/jp201919r.